Published in IET Microwaves, Antennas & Propagation
Received on 12th December 2007
Revised on 1st June 2008
doi: 10.1049/iet-map:20070314

ISSN 1751-8725

Passive intermodulation in printed lines: effects of trace dimensions and substrate

A.P. Shitvov D.E. Zelenchuk A.G. Schuchinsky V.F. Fusco

The Institute of Electronics, Communications and Information Technology (ECIT), Northern Ireland Science Park, Queen's University of Belfast, Queen's Road, Queen's Island, BT3 9DT Belfast, Northern Ireland, UK
E-mail: a.schuchinsky@qub.ac.uk

Abstract: A comprehensive experimental study was performed to identify and discriminate mechanisms contributing to passive intermodulation (PIM) in microstrip transmission lines. The effects of strip length and width, and substrate materials on PIM performance of printed lines were investigated in the GSM900, DCS1800 and UMTS frequency bands. The major features of the experiment design, sample preparation and test setup are discussed in detail. The measurement results have demonstrated that the PIM level cumulatively grows on the longer microstrip lines and decreases on wider strips and, thus, indicated that the distributed resistive nonlinearity of the printed traces represents the dominant mechanism of intermodulation generation in the printed lines on PTFE-based substrates.

1 Introduction

Printed circuit boards (PCBs) constitute the backbone of most telecommunication equipment. The signal integrity and electromagnetic compatibility of the PCB-based devices impose increasingly stringent requirements to PCB performance and pose particular challenges in high-power applications such as printed antennas, filters and interconnects [1].

Passive intermodulation (PIM) in printed circuits has major detrimental effects leading to deleterious electromagnetic interference in wireless communications systems. Despite the growing demand for effective means of mitigating PIM generation in PCBs, the mechanisms underlying this phenomenon are still barely understood and are scarcely addressed in the technical literature.

Recent studies [2–5] have revealed some correlation between the properties of PCB materials and measured PIM products. At the same time, they have also demonstrated that the PIM performance of printed traces was extremely sensitive to the measurement techniques and fabrication processes. Moreover, the results of the PIM measurements presented in the literature were often inconsistent, for example, the correlation between carrier attenuation and the PIM level reported in [2] was not observed in [3].

Nevertheless, certain interrelations between laminate construction and the PIM performance of processed PCB have been empirically identified [5]. In particular, the effect of the copper cladding and the surface bonding layer on PIM performance has been observed along with the effect of walls of etched traces [2, 4]. However, the role of the trace shape and laminate composition in PIM production has received no consistent interpretation so far, mostly because of lack of the pertinent experimental data on PIM generation in PCB materials.

To address these issues and gain insight into the origins of PIM production in PCB materials, it is essential to perform systematic and repeatable PIM measurements on the canonical printed structures, which are adequately described by the predictive phenomenological models. Therefore the objective of this study was to set up the targeted experiments, which could allow us to measure PIM products on the microstrip lines and juxtapose the obtained experimental data with the characteristics inferred from the nonlinear transmission line (NTL) model [6, 7].

doi: 10.1049/iet-map:20070314

In this paper, we present the results of the first comprehensive experimental study of third-order PIM (PIM3) generation on microstrip lines specially designed and manufactured in order to identify and separate the individual contributions of the material and geometrical parameters to PIM performance of PCB. The main features of the PIM characterisation of PCB materials, the test setup and data analysis are presented in Section 2. In Section 3, the results of the PIM measurements are discussed, and the main findings are summarised in the Conclusions. The principal aspects of the NTL model used for interpretation of the PIM measurements are summarised in Appendix.

2 Design of experiments

2.1 Measurement setup

The test setup is based on a commercial Summitek Instruments PIM analyser [8]. Three different models: SI-900B, SI-1800B and SI-2000B(E), have been used for the measurements in the GSM900, DCS1800 and UMTS frequency bands as detailed in Table 1. The analyser feeds a two-tone signal (two continuous wave carriers) into the device under test (DUT), and monitors levels of the forward PIM products at the DUT output port and the reverse PIM products at the DUT input port in the respective bands of the instrument receiver. Magnitude of the forward and reverse PIM3 products (P_{IM3}) is measured either at a spot frequency or in a frequency sweep of one tone at a time. In the latter case, the PIM3 frequency $f_{IM3} = 2f_1 - f_2$ ($f_1 < f_2$) is swept in the bands specified in Table 1 as follows:

1. The carrier frequency f_1 is fixed at its lowest value, and f_2 is swept downward from its maximum value (referred to as 'DOWN' sweep).

2. The carrier frequency f_2 is fixed at its maximum value, and f_1 is swept upward from its lowest value (referred to as 'UP' sweep).

To ensure a meaningful comparison of test specimens, the full test setup is first calibrated for the residual P_{IM3} level without a DUT. This provides a reference P_{IM3} level of the test instrument together with the cable assemblies. The measurement uncertainty has been assessed by repeating the tests after disconnecting and reconnecting the DUT three to five times and then averaging the measurement results over the swept frequency band and a series of reconnections. This allows us to reduce the effect of intrinsic noise in the test setup itself, which could be commensurate with the measured P_{IM3} level in high-quality (low PIM) PCB laminates. Therefore the mean values of the measured P_{IM3} are adopted in this paper as the representative quantities for characterisation of specimen performance. The viability of such an approach is supported by the following observations:

i. The P_{IM3} levels at spot frequencies demonstrated time variations whereas their median consistently remained within narrow margins.

ii. Frequency dependencies of P_{IM3} magnitude exhibited random kinks, especially, the reverse P_{IM3} response. These could be caused by occasional minor changes in the sample assembly or drift of the instantaneous residual P_{IM3} level. Such adverse effects of the instrumental instabilities were grossly eliminated by averaging.

Finally, it is important to note that the instrument uncertainties strongly affect measurement data at the level close to the residual PIM level [8]. However, our extensive tests have shown that even near the analyser sensitivity floor, where the instantaneous P_{IM3} level has greater variations, the P_{IM3} median consistently demonstrates the distinctive signatures of PIM products in the test specimens.

2.2 Sample design and preparation

The board layouts with the microstrip line specimens used in the experiments are shown in Fig. 1, and the parameters of the respective PCB materials are listed in Table 2. The test samples were specially designed to explore the effects of trace geometry and substrate material composition on PIM3 generation. To reduce sensitivity of the test results to manufacturing factors and tolerances, two to three replicas of each board were fabricated simultaneously. The following microstrip line specimens were manufactured and tested:

Table 1 Frequency bands of carriers and PIM3 products

PIM analyser	Frequency band	Frequency sweep	f_1, MHz	f_2, MHz	f_{IM3}, MHz
SI-900B	GSM900	DOWN	935	960–955	910–915
		UP	935–937.4	960	910–914.8
SI-1800B	DCS1800	DOWN	1832–1805	1880	1784–1730
		UP	1805	1880–1825	1730–1785
SI-2000B(E)	UMTS	DOWN	2110	2170–2160	2050–2060
		UP	2110–2115	2170	2050–2060

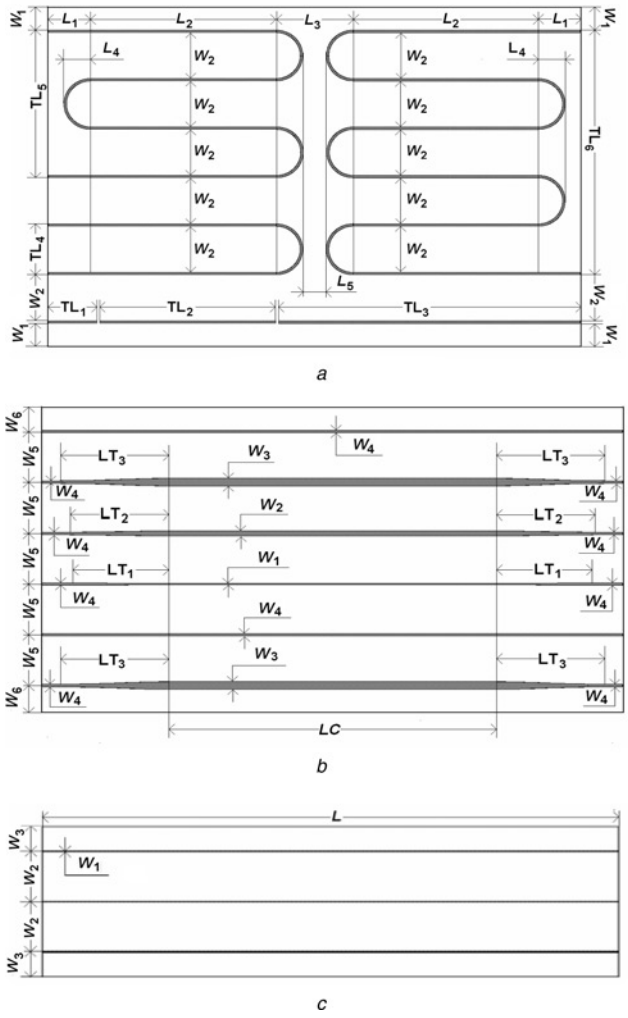

Figure 1 *Plan view of the microstrip lines on the boards specified in Table 2*

a Layout of Board 1 – uniform straight and meandered microstrip lines of different lengths (width of all traces is 4.32 mm): 100 mm (TL_1), 300 mm (TL_2), 500 mm (TL_3), 917 mm (TL_4), 1828 mm (TL_5), 2736 mm (TL_6); other dimensions: $W_1 = 41.4$ mm, $W_2 = 82.7$ mm, $L_1 = 72.1$ mm, $L_2 = 318$ mm, $L_3 = 132.9$ mm, $L_4 = 45.7$ mm, $L_5 = 40.6$ mm

b Layout of Boards 2 and 3 with microstrip lines of different widths: $W_1 = 2.29$ mm, $W_2 = 9.14$ mm, $W_3 = 13.46$ mm, $W_4 = 4.32$ mm; length of the uniform central sections: $LC = 522$ mm; lengths of the tapered sections: $LT_1 = 164.8$ mm, $LT_2 = 169.6$ mm, $LT_3 = 186.7$ mm; full length of the trace: $L = 914$ mm; distance between traces: $W_5 = 87$ mm; distance from the edge: $W_6 = 43.5$ mm

c Layout of Boards 4–9 with straight uniform 50 Ω microstrip lines of length $L = 914$ mm on different substrates; the substrate parameters and the respective strip widths W_1 for each material are given in Table 2; distance between traces: $W_2 = 87$ mm; distance from the edge: $W_3 = 43.5$ mm

i. Uniform straight and meandered 50 Ω lines of several lengths (Board 1 with the layout shown in Fig. 1*a*).

ii. Straight lines of different widths combined with the six-section Klopfenstein tapered transformers providing the impedance matching between the central sections and 50 Ω input/output ports (Boards 2 and 3 with the layout shown in Fig. 1*b*).

iii. Straight uniform 50 Ω microstrip lines on the substrates with different laminate compositions (Boards 4–9 specified in Table 2 with the trace layouts shown in Fig. 1*c*).

Note that the Boards 1–3 are made of the same laminate material, see Table 2.

The PIM measurement data available from the PCB manufacturers and end-users often showed significant variations of PIM3 performance of printed lines despite their substrate materials having identical specifications, [4, 5]. To minimise uncertainties caused by the different raw materials in PCB laminates and fabrication techniques, our specimens were produced in strictly controlled manufacturing processes. Namely, Boards 1–3 and 9 have the same laminate composition and copper cladding but different thickness. The same grade of low-profile reverse-treated copper foil of thickness 35 μm with metallic zinc-free anti-tarnish coating was used for copper cladding of all laminates except Board 4. The foil used in Board 4 had the same thickness but came from a different supplier. To prevent environmental contamination of the exposed copper surfaces, all conductors were coated by a 1 μm thick immersion tin. According to [9], such a protective layer provides low PIM finishing of the printed traces. The specimens were manufactured by the same commercial PCB processing house and produced in three separate batches: (i) Boards 1 (ii) Boards 2 and 3 and (iii) Boards 4–9.

2.3 Microstrip launchers

The low-PIM launchers represent the critical elements of the test setup employed for evaluation of PIM performance of PCB laminates. It was shown experimentally in [10] and is corroborated experimentally in Section 3.4 below that input/output matching of the printed microstrip lines has a significant impact on the measured PIM3 response of the transmission lines. Therefore high-quality coaxial-to-microstrip transitions are required to reduce the inhomogeneity of the power distribution along the traces, which is caused by standing waves in the mismatched lines. The board launchers have been specially designed for our experiments to provide the reflection coefficient less than −20 dB over a wide frequency range (broadband matching is necessary for testing the same specimens in the different frequency bands).

To examine the effect of the launchers on the PIM3 generation, the straight uniform microstrip lines on Boards 4–7 were equipped with two types of coaxial-to-microstrip transitions shown in Fig. 2:

i. Cable launchers, Fig. 2*a*, were made from the PIM3 certified connectorised cable assemblies, which comprised

doi: 10.1049/iet-map:20070314

Table 2 Boards specifications and the material parameters

Board number	Dielectric composition	Thickness, mm	Relative permittivity	Loss tangent	Strip width of 50 Ω line, mm
1–3	PTFE/woven glass	1.58	2.5[a]	0.0019[a]	4.32
4[b]	Cured resin-impregnated woven glass	0.76	3.00[a]	0.0034[a]	1.9
5	PTFE/woven glass	0.76	3.00[a]	0.0030[a]	1.9
6	BT epoxy/ceramic/woven glass	0.76	3.00[a]	0.0026[a]	1.9
7	PTFE/ceramic/woven glass	0.76	3.00[c]	0.0014[c]	1.9
8	PTFE/woven glass	0.76	2.17[a]	0.0009[a]	2.3
9[d]	PTFE/woven glass[d]	0.76	2.5[d]	0.0019[d]	2.11

[a]Measured at 10 GHz [b]Different supplier of raw copper foil and laminate [c]Measured at 1.9 GHz [d]Boards 1-3 and 9 have similar laminate composition

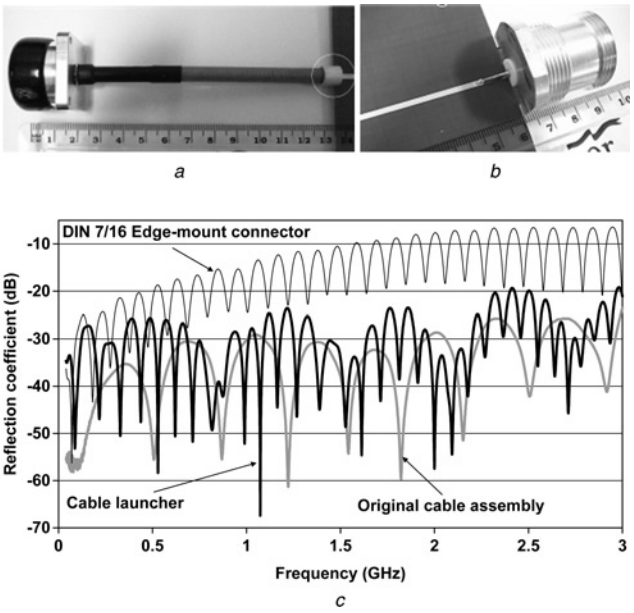

Figure 2 *Microstrip launchers*

a Cable launcher
b DIN 7/16 edge-mount connector
c Input reflection coefficient of the cable launchers and connectors, measured on Board 6, and the original cable assembly used for making the cable launchers

6.35 mm semi-rigid coaxial cable of length 250 mm and DIN 7/16 flange-mount connectors. The cable assemblies were cut in the middle and each half was fitted at the PCB edges using the newly designed coaxial-to-microstrip adaptors (see the encircled item in Fig. 2*a*).

ii. DIN 7/16 edge-mount connectors were attached directly at the PCB edges; see Fig. 2*b*. The measurement results in Fig. 2*c* demonstrate that the cable launchers exhibit a considerably lower reflection coefficient than the edge-mount connectors: less than −25 dB in the GSM900 frequency band and −20 dB in the DCS1800 and UMTS bands.

Finally, it is important to note that this study was carried out on high-performance PCB materials certified by manufacturers for low-PIM applications. Consequently, PIM characterisation of such materials poses an enormous challenge because of the limited sensitivity of the available PIM analysers (typically −125 dBm over 90% of the intermodulation frequency band), and the difficulties in separating PIM products generated by the printed traces and the test fixture including launchers/connectors. Nonetheless, the results presented in Section 3 demonstrate that the experimental approach described here provides a consistent and reliable means for evaluation of PIM performance of a broad range of PCB materials.

3 Experimental results and discussion

The test specimens described in Section 2 have been designed for the targeted experiments, which are aimed at identification of the PIM generation mechanisms in microstrip lines and discrimination of the effects of trace geometry and the substrate material on PIM performance of PCB laminates.

All measurements were performed in a screened anechoic chamber to exclude interference from external sources. After each reconnection of the specimen, the integrity of the whole assembly was checked by tapping the joints and the board to ensure that there were no mechanical faults or loose connectors, which could alter PIM response of the DUT. Occasionally during the tests, we observed a drift of carrier(s) power that led the P_{IM3} magnitude of the DUT to fall below the initial residual level. Such instances were treated as random errors of the instrument and were included in the estimations of the measurement uncertainty.

3.1 Cumulative effect

Distributed weak nonlinearity of the printed traces has been assumed as a primary source of PIM generation in microstrip

lines on low-loss substrates. The NTL model [7] with the current-driven nonlinear resistivity defined by (1) in Appendix predicted cumulative growth of the forward P_{IM3} with line length. To investigate this phenomenon experimentally, P_{IM3} level on the uniform 50 Ω microstrip lines of several different lengths was measured first. Magnitude of the forward P_{IM3} on the microstrip traces of Board 1 (Fig. 1*a*) is shown in Fig. 3 for the 'DOWN' frequency sweep in the DCS1800 band. The plotted experimental points represent mean values in the swept frequency band (1730–1784 MHz), and the error bars delimit the maximum P_{IM3} deviations in the series of reconnections.

Fig. 3 demonstrates that forward P_{IM3} monotonically grows on the longer traces, and the measurement results correlate well with the NTL model prediction based on (2). The measurement results of the same lines for the GSM900 band were reported earlier in [11] and also exhibited a general trend of higher forward P_{IM3} on longer traces. In the 'UP' frequency sweep, Table 1, the forward P_{IM3} level exhibits the same qualitative trend, although its magnitude differs slightly. This discrepancy is attributed to dissimilar matching conditions in the 'UP' and 'DOWN' sweeps of the respective carrier frequencies (Fig. 2*c*). It is noteworthy that despite a steady increase of the forward P_{IM3} with line length in Fig. 3, it does not grow indefinitely. According to the NTL model, when attenuation of the carriers on sufficiently long lines exceeds the rate of P_{IM3} generation, forward P_{IM3} starts to decay (2). This phenomenon was also observed in the theory of travelling-wave harmonic generators [12].

In contrast to the forward P_{IM3}, the reverse P_{IM3} level showed no consistent increase on longer lines, and its level remained below the forward P_{IM3}. These observations are consistent with the NTL model predictions and suggest that the reverse PIM products are predominantly formed near the input port of the matched microstrip line. This effect can also be attributed to the phase matching in a nonlinear mixing process [13].

Thus, the presented results of P_{IM3} measurements on microstrip lines of different lengths provide conclusive evidences of the cumulative growth of PIM3 products on printed lines [2, 14] and support the phenomenology of the NTL model with distributed nonlinearity.

3.2 Effect of strip width

The effect of strip width on PIM3 product generation is difficult to assess independently because it is accompanied by the line mismatch, which is caused by the change of the line impedance. Two approaches have been used to investigate this effect:

i. Substrates with modified parameters to compensate for the strip width variations and maintain the line impedance at the 50 Ω [3].

ii. Impedance transformers integrated with lines of different widths on the same substrate to provide matching to 50 Ω input and output ports (Fig. 1*b*).

The latter configuration has been adopted in this work because it allows the direct comparison of the lines of several different widths on a single board (Fig. 1*b*) and, thus, excludes additional uncertainty incurred by dissimilar substrates. The shortcoming of this arrangement is that the matching transformers may also contribute to PIM3 generation and somewhat obscure the effect of the line width as detailed below.

The results of forward P_{IM3} measurements in the GSM900 frequency band are shown in Fig. 4 for the matched microstrip lines of several widths fabricated on

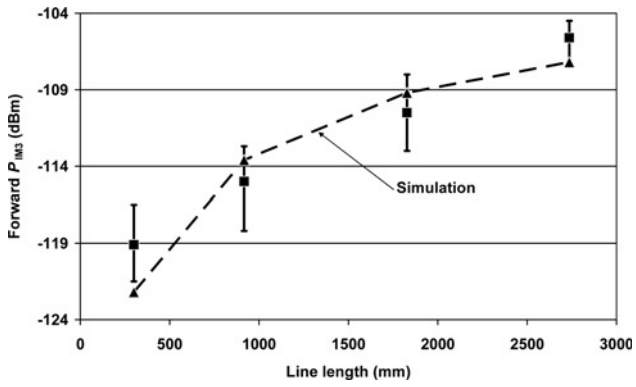

Figure 3 *Forward P_{IM3} against the line length measured on Board 1 (squares) in the DCS1800 band ('DOWN' sweep) at carriers' power 2 × 43 dBm and the NTL model simulations at 1730 MHz (triangles)*

Error bars delimit the maximum P_{IM3} deviations in the series of reconnections

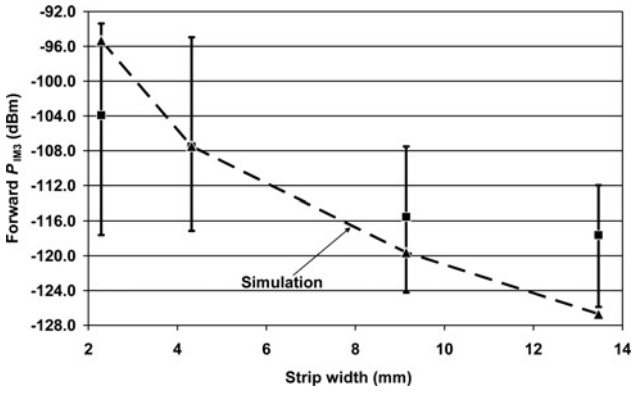

Figure 4 *Forward P_{IM3} against microstrip line width measured on Boards 2 and 3 (squares) in the GSM900 band ('UP' sweep) at carriers' power 2 × 43 dBm, and the NTL model simulations at 910 MHz (triangles)*

Error bars delimit the maximum P_{IM3} deviations within each group of the specimens with the same strip width

doi: 10.1049/iet-map:20070314

Boards 2 and 3 (see the layout in Fig. 1*b*). The data points in Fig. 4 represent quantities averaged over the frequency band, the sample line triplets and a series of reconnections (the residual forward P_{IM3} level was below −120.4 dBm). Error bars delimit the maximum P_{IM3} deviations within each group of specimens with the same strip width.

The P_{IM3} magnitude in Fig. 4 exhibits a monotonic decrease with strip width that can be attributed to lower current density on wider traces with nonlinear resistivity defined by (1). A similar effect was also observed in [3] for microstrip lines with different substrates. These experimental results are consistent with NTL model predictions and, hence, provide an independent confirmation that the current-driven distributed nonlinear resistivity of printed traces represents the dominant mechanism of PIM3 generation in microstrip lines on PTFE/woven glass substrates.

It is noteworthy that the forward P_{IM3} magnitude measured on 917 mm long uniform microstrip lines on Boards 2 and 3 is higher than on Board 1, Figs. 3 and 4. The only difference between these two groups of specimens is that they were manufactured in separate batches. This fact demonstrates once again that PIM performance of printed lines is highly sensitive to the laminate materials and fabrication process.

The reverse P_{IM3} level has shown little correlation with the strip width. Apparently, this implies that weakly reflecting matching transformers make a dominant contribution to the reverse P_{IM3}. This conclusion is consistent with the observations in Section 3.1 that the reverse P_{IM3} level is predominantly determined by the line section near the input port of the matched microstrip line, and that even small reflections can noticeably affect the reverse P_{IM3} [11]. This is why impedance matching transformers may completely disguise the effect of the trace width on the reverse P_{IM3} level.

It is necessary to note that P_{IM3} measurements on the traces of different widths have shown higher sensitivity to fabrication tolerances and workmanship, which cause higher measurement uncertainties, Fig. 3. Nevertheless, the obtained experimental results consistently demonstrate the qualitative trend of a lower forward P_{IM3} on microstrip lines with wider traces. These results provide further evidence of PIM generation on Boards 1–3 by the current-driven distributed nonlinearity of printed traces (Appendix).

3.3 Effect of dielectric substrate

The effect of the dielectric substrate on PIM3 generation in the GSM900 frequency band had been first considered in [11]. In this section, the study is substantially extended to include other frequency bands and different materials and to investigate, particularly, the relationship between the dielectric substrate loss and P_{IM3} level.

To evaluate the effect of laminate composition on PIM3 performance of PCB, straight uniform 50 Ω microstrip lines were fabricated on Boards 4–9 (Fig. 1*c*), whose parameters are given in Table 2 (manufacturers' specifications). The insertion loss in each line was measured first at frequencies 910, 1730 and 2050 MHz and is plotted against the substrate loss tangent in Fig. 5*a* (zero loss tangent corresponds to the typical cable assembly used for making the cable launchers). The results of forward P_{IM3} measurements in the GSM900, DCS1800 and UMTS bands are shown in Fig. 5*b*. The experimental points represent mean values in the respective frequency bands averaged over the sample triplets. The value at 0 loss tangent corresponds to the residual forward P_{IM3} of the PIM analyser with the test fixture.

Although a general trend of increased PIM production on the boards with higher permittivity and loss tangent can be inferred from Fig. 5, no consistent correlation between the P_{IM3} level and the substrate loss has been observed. Indeed, comparison of the linear insertion loss in Fig. 5*a* and P_{IM3} level in Fig. 5*b* shows that although insertion loss grows with loss tangent, P_{IM3} magnitude does not follow the same trend. This implies that for tested laminates, dielectric loss represents a second-order effect on PIM3

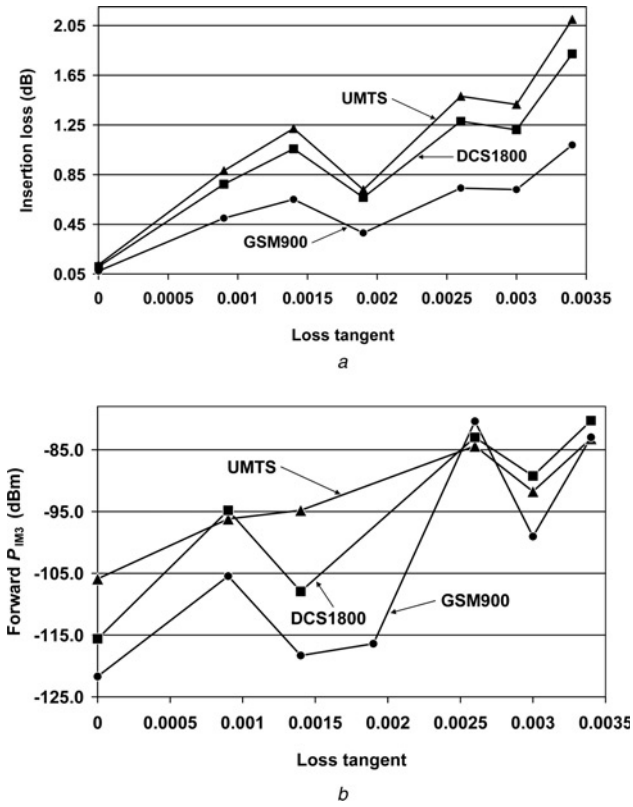

Figure 5 *Insertion loss and forward P_{IM3} against the substrate loss tangents specified in Table 2*

a Insertion loss at f_{IM3} frequencies of 910 MHz (GSM900, circles), 1730 MHz (DCS1800, squares) and 2050 MHz (UMTS, triangles)
b Forward P_{IM3} at carriers' power 2 × 43 dBm in GSM900 (circles), DCS1800 (squares) and UMTS (triangles) frequency bands

Table 3 P_{IM3} against dielectric substrate parameters measured at $f_{IM3} = 910$ MHz and carriers' power 2 × 43 dBm

Board number	Relative permittivity	Loss tangent	Forward 'UP' P_{IM3}, dBm	Reverse 'UP' P_{IM3}, dBm
8	2.17	0.0009	−104.8	−122.3
9	2.5	0.0019	−115.7	−126.2
5	3.0	0.0030	−97.7	−126.5

generation when compared with the nonlinear resistivity of printed traces. Apparently, various ingredients of the laminate composition such as glass reinforcement, bonding layers, impregnation and others affect the P_{IM3} level through both nonlinearity of the substrate itself and the linear attenuation of carriers caused by the dielectric loss (2). However, individual contributions of these two mechanisms can hardly be separated in our two-port measurements.

The results of P_{IM3} measurements at $f_{IM3} = 910$ MHz on Boards 5, 8 and 9 with similar laminate composition (Table 2) are summarised in Table 3. In contrast to other substrates, these laminates are composed of PTFE and woven glass only and do not contain any additives. Their main differences consist in the grade of glass reinforcement and bonding layers. However, despite the similarity of the laminate construction and the constituent materials used, no explicit correlation between the forward P_{IM3} level and substrate permittivity or loss tangent has been observed. The level of the reverse P_{IM3} also remains practically unchanged (note that the reverse P_{IM3} level in Table 3 is commensurate with the background P_{IM3} of the entire test setup whose sensitivity floor is limited not only by the reverse residual P_{IM3} of the instrument itself (measured at −132 dBm) but also by the test fixture, cable launchers and connectors). Then, taking into account that the same copper cladding was used in all these specimens, we can infer that the observed differences in PIM3 performance of the tested laminates are inflicted by the weak intrinsic nonlinearity of dielectric substrates. This phenomenon requires further experimental and theoretical investigations and will be addressed elsewhere.

Table 4 Forward and reverse P_{IM3} (dBm) on the Boards 4–7 with the cable launchers and DIN 7/16 edge-mount connectors; the measurement results for the UMTS band at carriers' power 2 × 43 dBm

Board number	Cable launchers		DIN 7/16 edge-mount connectors	
	Forward P_{IM3}	Reverse P_{IM3}	Forward P_{IM3}	Reverse P_{IM3}
4	−83.2	−98	−82.1	−86.1
5	−91.8	−108.7	−90.2	−95
6	−84.4	−104.4	−85.8	−99.1
7	−94.8	−102.5	−89.9	−91.5

3.4 Effect of impedance matching

The effect of impedance matching on PIM3 generation by microstrip lines has been evaluated with two types of microstrip launchers shown in Fig. 2: cable launchers and edge-mount connectors. The results of P_{IM3} measurements in the UMTS band are summarised in Table 4 and demonstrate that regardless of the board type, the specimens with edge-mount connectors typically exhibit reverse P_{IM3} of an order ~5–10 dB higher than samples with cable launchers. The forward P_{IM3} remains nearly at the same level for both types of launchers, being primarily determined by the properties of the substrate and traces. The observed effect of impedance mismatch on P_{IM3} is fully consistent with the simulation results [10] obtained from the NTL with distributed nonlinear resistivity.

Indeed, according to [10], the load mismatch more strongly affects the reverse P_{IM3} level than the forward P_{IM3}, whereas the reverse P_{IM3} level remains always lower than the forward P_{IM3}. This is exactly what has been observed in all our measurements, and it is also consistent with the measurement results discussed in Section 2.3. Thus, we can infer from these experimental observations that high quality matching is a prerequisite for reliable and consistent evaluation of PIM3 performance of printed circuits and PCB materials.

4 Conclusions

The targeted experiments have been carried out to identify the mechanisms of PIM generation on printed microstrip lines and to elucidate the effects of the trace geometry and material parameters on PIM3 performance of PCB laminates. To ensure the integrity of the measurements, the microstrip lines were thoroughly designed and fabricated using controlled manufacturing processes. Special cable launchers with a low reflection coefficient (less than −20 dB) over a broad frequency band have been designed to provide the high quality impedance matching of the specimens with the test instruments. In the measurement trials, the effects of strip length and width, substrate material and launchers on PIM3 generation in microstrip lines have been explored. The main findings can be summarised as follows:

i. The magnitude of the forward P_{IM3} monotonically increases with line length, thus providing explicit evidences of the cumulative growth of the PIM3 products along the line caused by the distributed nonlinearity of the printed traces.

IET Microw. Antennas Propag., 2009, Vol. 3, Iss. 2, pp. 260–268
doi: 10.1049/iet-map:20070314

ii. The reverse P_{IM3} level is lower than the forward P_{IM3} on the matched lines and shows no direct correlation with line length; however, the reverse PIM3 is more strongly affected by the impedance mismatch.

iii. The average magnitudes of the forward P_{IM3}, measured on Boards 2 and 3, exhibit a monotonic decrease with line width; this observation along with the cumulative growth of PIM products suggest that the current-driven distributed nonlinearity of microstrip traces represents the dominant mechanism of PIM generation on printed lines.

iv. For tested PCB laminates, no obvious correlation has been observed between the measured P_{IM3} level and the permittivity, loss tangent and composition of the substrates; these results indicate that nonlinearity of the PTFE-based substrates represents a second-order effect when compared with nonlinear resistivity of the printed traces.

v. Input/output matching significantly affects the generation of the reverse P_{IM3}, namely, edge-mount connectors typically exhibit the reverse P_{IM3} level of $\sim$5–10 dB higher than cable launchers, whereas the level of forward P_{IM3} remains nearly the same for both the types of launchers.

The study of PIM generation on printed lines presented in the paper is based on measurements, which involved multiple samples of different lengths and shapes. Alternatively, near-field probing can be employed to map PIM product distributions on printed traces. This approach has recently been implemented in [15] and has independently confirmed the cumulative growth of the forward P_{IM3} level on microstrip lines. However, it is necessary to note that near-field probing on low-PIM laminates and short transmission lines is constrained by the sensitivity floor of the PIM analysers and the requirement of a weak coupling of the probe (typically less than -35 dB). Thus, the two-port PIM measurements used in this paper currently represent the only practical way for characterisation of the high performance PCB materials with low intrinsic nonlinearity.

5 Acknowledgment

The authors are grateful to Taconic Advanced Dielectric Division Ltd., Trackwise Designs Ltd., Racal Antennas Ltd., PCTEL Inc. and Castle Microwave Ltd. for their generous help with the preparation of the test samples and providing measurement facilities. Special thanks to Mr. Jim Francey for numerous discussions and support. The authors appreciate the suggestions made by Dr. David Linton over the period of this work.

6 References

[1] MCCARTHY T.F., MORRELL M., TRIPI J.: 'Signal integrity measurements support the candidacy of PTFE at high data rates'. Proc. High-Performance System Design Conf. (DesignCon 2003), Santa Clara, CA, USA, January 2003 HP3-6

[2] SCHUCHINSKY A.G., FRANCEY J., FUSCO V.F.: 'Distributed sources of passive intermodulation on printed lines'. Proc. 2005 IEEE Antennas and Propagation Society Int. Symp., Washington, DC, USA, July 2005, vol. 4B, pp. 447–450

[3] KUGA N., TAKAO T.: 'Passive intermodulation evaluation of printed circuit board by using 50 Ω microstrip line'. Proc. Asia Pacific Microwave Conf. (APMC 2004), New Delhi, India, December 2004

[4] EL BANNA B.: 'Passive intermodulation from printed circuit boards'. Technical Report D1200002735, Powerwave Technologies, Inc., Sweden, June 2006

[5] FRANCEY J.: 'Passive intermodulation study' Technical Report, Taconic ADD, 2003, http://www.taconic-add.com, accessed April 2008

[6] SHITVOV A.P., ZELENCHUK D.E., SCHUCHINSKY A.G.: 'Distributed model of passive intermodulation phenomena in printed transmission lines'. Proc. 13th Int. Student Seminar on Microwave Applications of Novel Physical Phenomena, Rovaniemi, Finland, August 2006, pp. 61–63

[7] ZELENCHUK D.E., SHITVOV A.P., SCHUCHINSKY A.G., OLSSON T.: 'Passive intermodulation on microstrip lines'. Proc. 37th European Microwave Conf. (EuMC'07), Munich, Germany, October 2007, pp. 396–399

[8] Passive intermodulation distortion analyzer: 'Operating and maintenance manual'. Summitek Instruments, Part Number 1902000, Rev. C, June 2004 edn.

[9] PEREZ J.V.S., ROMERO F.G., RÖNNOW D., SÖDERBÄRG A., OLSSON T.: 'A micro-strip passive inter-modulation test set-up; comparison of leaded and lead-free solders and conductor finishing'. Proc. 5th Int. Workshop on Multipactor, Corona and Passive Intermodulation in Space RF Hardware (MULCOPIM 2005), Noordwijk, The Netherlands, 2005, pp. 215–222

[10] ZELENCHUK D.E., SHITVOV A.P., SCHUCHINSKY A.G.: 'Effect of matching on passive intermodulation in transmission lines with distributed nonlinear resistance'. Proc. Int. URSI Commission B – Electromagnetic Theory Symp. (EMTS 2007), Ottawa, ON, Canada, July 2007, R19-39, EMTS171

[11] ZELENCHUK D.E., SHITVOV A.P., SCHUCHINSKY A.G.: 'Effect of laminate properties on passive intermodulation generation'. Proc. Loughborough Antennas and Prop. Conf. (LAPC 2007), Loughborough, UK, April 2007, pp. 169–172

[12] AULD B.A., DIDOMENICO M. JR., PANTELL R.H.: 'Traveling-wave harmonic generation along nonlinear transmission lines', *J. Appl. Phys.*, 1962, **33**, (12), pp. 3537–3545

[13] SHITVOV A.P., ZELENCHUK D.E., SCHUCHINSKY A.G.: 'Experimental observations of distributed nonlinearity in printed lines'. Proc. 14th Int. Student Seminar on Microwave and Optical Applications of Novel Physical Phenomena, Belfast, UK, 2007, pp. 70–73

[14] SHITVOV A.P., ZELENCHUK D.E., SCHUCHINSKY A.G., FUSCO V.F.: 'Studies on passive intermodulation phenomena in printed and layered transmission lines'. Proc. 10th High Frequency Postgraduate Student Colloquium, Leeds, UK, 2005, pp. 7–10

[15] SHITVOV A.P., ZELENCHUK D.E., SCHUCHINSKY A.G., FUSCO V.F., BUCHANAN N.: 'Mapping of passive intermodulation products on microstrip lines'. Proc. 2008 IEEE MTT-S Int. Microwave Symp., Atlanta, GA, June 2008, THP2H-02

[16] SERON D., COLLADO C., MATEU J., O'CALLAGHAN J.M.: 'Analysis and simulation of distributed nonlinearities in ferroelectrics and superconductors for microwave applications', *IEEE Trans. Microw. Theory Tech.*, 2006, **54**, (3), pp. 1154–1160

[17] DAHM T., SCALAPINO D.J.: 'Theory of intermodulation in superconducting microstrip resonator', *J. Appl. Phys.*, 1997, **81**, (4), pp. 2002–2009

[18] ILYNSKY A.S., SLEPYAN G.Y., SLEPYAN A.Y.: 'Propagation, scattering and dissipation of electromagnetic waves' (Peter Peregrinus Ltd., London, 1993)

7 Appendix

A phenomenological model of PIM3 generation in printed transmission lines with a weak distributed nonlinearity [6, 7] is used to interpret the measurement results. The current-driven per-unit-length nonlinear resistance is defined similar to [16, 17]

$$R = R_0 + R_2 I^2 = \rho_0 \frac{\int J^2 \, \mathrm{d}s}{\left(\int J \, \mathrm{d}s\right)^2} + \rho_2 \frac{\int J^4 \, \mathrm{d}s}{\left(\int J \, \mathrm{d}s\right)^4} I^2; \quad R_0 >> R_2 I^2 \tag{1}$$

where R_0 is the linear resistance and R_2 the nonlinear resistance; J is the surface current density on the infinitesimally thin imperfect conductors, [18]; ρ_0 and ρ_2 are the macroscopic linear and nonlinear resistivities, respectively. The macroscopic nonlinear resistivity ρ_2 is the model parameter, which is retrieved from the experimental data.

The solution of the nonlinear telegrapher's equations for the perfectly matched segment of the transmission line of finite length l gives the following expression for the current distribution along the line at the PIM3 frequency f_{IM3} [7]

$$I_{\mathrm{IM3}}(x) = R_2 \xi [-(1+\nu)\exp(-\gamma_{\mathrm{IM3}} x) + \exp(-(2\gamma_1 - \gamma_2)x) + \nu \exp(-\gamma_{\mathrm{IM3}}(2l - x) - 2\alpha l)] \tag{2}$$

where $\gamma_{1,2,\mathrm{IM3}} = i\beta_{1,2,\mathrm{IM3}} + \alpha$ are the complex wavenumbers at the frequencies of carriers $f_{1,2}$ and of the intermodulation product f_{IM3}; $\xi = 3V_1^2 V_2 / \left[32\nu Z_0^2(f_1) Z_0(f_2) Z_0(f_{\mathrm{IM3}}) \times (\gamma_{\mathrm{IM3}} + \alpha)\right]$, $\nu = \alpha/\gamma_{\mathrm{IM3}}$ and $V_{1,2}$ are the source voltages at the frequencies $f_{1,2}$ and $Z_0(f)$ is the line characteristic impedance. Then, forward P_{IM3} magnitude is calculated as follows

$$P_{\mathrm{IM3}}(l) = \frac{1}{2}\mathrm{Re}\left\{I_{\mathrm{IM3}}(l) U_{\mathrm{IM3}}(l)^*\right\} \tag{3}$$

where $I_{\mathrm{IM3}}(l)$ and $U_{\mathrm{IM3}}(l)$ are current and voltage at the transmission line output ($x = l$); * stands for complex conjugation and Re{} is the real part. Equations (1)–(3) are used for calculations of the P_{IM3} level on microstrip lines with the dominant current-driven nonlinearity.

doi: 10.1049/iet-map:20070314